

THE ROLE OF TRANSITION MODELING IN CFD PREDICTIONS OF STATIC AND DYNAMIC STALL

Marvin A. Moulton

marvin.moulton@us.army.mil

US Army Research, Development and Engineering Command
Huntsville, AL, 35898-5000, USA

Tin-Chee Wong

tinchee.wong@us.army.mil

Marilyn J. Smith

marilyn.smith@ae.gatech.edu

School of Aerospace Engineering, Georgia Institute of Technology
Atlanta, Georgia, 30332-0150, USA

Arnaud Le Pape

Arnaud.Lepape@onera.fr

ONERA, The French Aerospace Lab
F-92190, Meudon, FRANCE

Jean-Claude Le Balleur

Jean-Claude.Leballeur@onera.fr

ONERA, The French Aerospace Lab
F-92322, Châtillon, FRANCE

Abstract

Advanced concepts such as high-speed rotors and rotors with active control have the potential to transform the rotorcraft industry through the improvement of rotorcraft performance and the reduction of vibration and noise. The design of these concepts, which involve non-linear aerodynamic and aeroelastic phenomena, requires high fidelity simulations, typically using computational fluid dynamics (CFD) methods. Dynamic stall on the retreating side of the rotor needs to be accurately captured if these new designs and concepts are to succeed. While recent advances in dynamic stall modeling with CFD have been presented in the past five years, the role of transition in CFD for both static and dynamic stall remains in question. A collaborative effort between the US and France is studying, in part, the ability of computational methods to predict dynamic stall. This paper will explore the use and efficacy of some transition models in the prediction of static and dynamic stall on the VR-7 airfoil. Experimental data are used for correlation of integrated loads, and viscous-inviscid solvers are used to aid in the characterization of the boundary layer in attached and separated static flows. Spatial and temporal studies previously carried out by the authors and others are leveraged to ensure that the results are independent of numerical artifacts. Numerical transition models have been observed to have minor impact on the prediction of the static and dynamic stall phenomena studied in this effort. Boundary layer convergence, with or without transition, appears to be a key component of the ability of the CFD methods to capture dynamic stall phenomena.

NOMENCLATURE

c = chord length, ft
 b = semi-chord length, ft
 C_d = drag coefficient
 C_f = skin friction coefficient
 C_ℓ = lift coefficient
 C_m = pitching moment coefficient, ref $1/4c$
 C_p = pressure coefficient
 k = reduced frequency, $k = \omega b / U_\infty$
 ℓ_{lam} = laminar separation bubble length
 M_∞ = freestream Mach number
 ω = frequency of oscillation, rad/sec
 n = integer
 Re = Reynolds number
 Re_{θ_s} = Re based on local boundary layer momentum thickness
 t = time, seconds
 T = period, seconds

U_∞ = freestream velocity, ft/sec
 x, y, z = Cartesian streamwise, radial and normal lengths, ft
 y^+ = dimensionless wall spacing
 α = angle of attack, deg

COMPUTER CODES

elsA = Navier-Stokes flow solver for structured multiblock and overset grids
 FUN3D = Navier-Stokes flow solver for unstructured grid, version 11.5
 OVERFLOW = Navier-Stokes flow solver for overset, structured grids, versions 2.1z and 2.2c
 VIS07 = RANS-Viscous-Inviscid Interaction solver
 XFOIL = interactive program for the design and analysis of subsonic isolated airfoils, version 6.94

INTRODUCTION

Computational studies on static and dynamic stall have experienced a resurgence in the past half decade thanks to the improved cost effectiveness of computational hardware and the advent of improved turbulence methods. Smith et al. [1], Sanchez-Rocha [2], Gleize et al. [3], and Szydowski and Costes [4] to name a few, have examined the ability of unsteady Reynolds Averaged Navier-Stokes (URANS) CFD to capture stall and post-stall characteristics of static airfoils and have studied grid dependence as well as turbulence modeling effects. Their conclusions note that turbulence modeling plays a key role in determining the stall characteristics, along with grids that are sufficient to resolve the boundary layer. The fully independent grid sizes recommended in some of these studies preclude application on engineering problems due to their restrictive size, and prediction of stall angle of attack and the accompanying coefficient magnitudes that include transition remains problematic.

These airfoil studies have been extended to include dynamic stall by a number of researchers. Studies on the convergence of dynamic stall have been carried out in various analyses, including, but not limited to Refs. 5–7. Similar conclusions to the static airfoil results have been observed. In some instances, errors in the prediction of the separation point resulted in a worsening of correlation with experiment as the mesh was refined. Mixed results with advanced turbulence models that include Large Eddy Simulation (LES) considerations have been observed. Again, some authors have concluded that the computational methods were not able to accurately reproduce the effects of dynamic stall with the resources available at the time. Physical (versus numerical) convergence analyses [7] and detailed investigation of experimental errors [8] have alleviated some of these concerns, but numerical predictions, in particular at low speeds where transition plays an important role, still have yet to be fully examined and improved.

This paper investigates the role of transition in static and dynamic stall through the use of current transition models, as well as an investigation into their influence on the physics of separation and reattachment. In addition to experimental data, viscous-inviscid interaction methods were employed to provide guidance and insight into understanding the transition predictions from the CFD methods.

EXPERIMENTAL DATA

The data used to validate the numerical predictions is contained in a three volume report [9–11]. An exhaustive summary of this test was given in Ref. [8]. Only a brief summary is provided below. The static and dynamic characteristics of eight airfoil sections (seven helicopter and a fixed-wing supercritical airfoil) were investigated in a 7×10 ft wind tunnel. This paper will only consider the VR-7 airfoil. The nominal range of flow conditions were as follows: freestream Mach numbers up to 0.30 and Reynolds numbers (based on chord) up to 4×10^6 . The 2 ft chord models were mounted vertically (from floor to ceiling) in the wind tunnel. The axis of rotation was located 4.9 ft downstream of the beginning of the constant-area section and at the midpoint of the 10 ft section

width. Rotation was about the quarter-chord.

Since the as-built airfoil ordinates were not available, the nominal data coordinates given in the report were utilized in this study. The boundary layer trip consisted of a 3 mm wide band of 0.1 mm diameter glass spheres glued to the leading edge. It is noteworthy that there was some conjecture from the authors of Ref. [9] that the presence of the pressure taps at critical locations may cause differences in transition and/or separation. The pressure transducers were Kulite YCQH-250-1 and YCQL-093-015 (smaller for leading and trailing edges) and were flush-mounted.

FLOW MODELING

Three CFD codes were utilized in this paper: elsA, FUN3D and OVERFLOW. Since all of the methodologies are well documented in the literature, only a brief summary of each method is given below. In addition, two viscous-inviscid interaction (VII) methods, VIS07 and XFOIL, were used to provide guidance and insight into the use of transition models in the CFD methods.

elsA Code

One of the URANS CFD methods used in the present study is the ONERA multi-application aerodynamic code elsA [12], which solves URANS equations for structured multi-block meshes in a finite-volume approach. For space discretization, the upwind AUSM+(P) scheme developed by Edwards and Liou [13] was used for the inviscid part of the fluxes while the viscous part uses a centered scheme. An interesting property of the AUSM+(P) scheme is that the numerical dissipation is proportional to the local velocity, so that it is low in the boundary layer. A second-order implicit method with LU factorization and Newton subiterations is used for the time discretization of the system. A wide range of turbulence models are available in elsA; in the present work, only the 2-equation $k - \omega$ model with Kok cross-derivative terms and the SST correction [14] was used.

Several transition criteria are available in elsA. In the present study, two of them were combined to provide transition locations along the airfoil. The first is the AHD stability criterion developed by Arnal et al. [15]. The second is the semi-empirical laminar bubble model proposed by Roberts [16,17] that provides an estimate of the length of the bubble based on the momentum thickness at the separation point and on the free stream turbulence level:

$$(1) \quad \frac{\ell_{lam}}{\theta_S} = 25,000 \frac{\log[\cotanh(0.1732 \cdot T_u)]}{Re_{\theta_S}}$$

This model was adjusted in order to match an LES simulation of the laminar bubble in the vicinity of static stall [18]. Validations of the model are presented in [19] and [6] for static and dynamic stall.

Numerical parameters as well as grid selection is based on an extensive study on the OA209 airfoil presented in [6]. For

the computations presented in this paper a 2D medium C-grid comprising 1,071x105 points was used over the airfoil and a H-grid comprising 61x53 points for the blunt trailing-edge. In case of unsteady computations for a pitching airfoil, a number of time steps per cycle of 36,000 is typically used together with a maximum number of 10 Newton subiterations to decrease the unsteady residual by 3 orders of magnitude.

FUN3D Code

FUN3D [20] is an unstructured URANS mesh flow solver and has been developed and supported by the NASA Langley Research Center. The Spalart-Allmaras [21] and Menter $k\omega$ -SST [14] turbulence models were used for the second-moment closure. The code uses an implicit, upwind, finite-volume discretization in which the dependent variables are stored at mesh vertices. Inviscid fluxes at cell interfaces are computed using a flux-differencing scheme, while viscous fluxes are evaluated by using an approach equivalent to a central-difference Galerkin procedure. For time-accurate computations, a generalized backward difference scheme is used to construct a higher-order temporal scheme by extending the difference stencil in time [22]. A temporal error control method is implemented as an exit criterion for the subiterative loop of the dual time stepping process. A maximum of thirty-five subiterations with 2,000 time steps per cycle to achieve an 8-order drop in magnitude of the turbulence residual was applied for these simulations with a specified fraction of 0.1 for temporal error control.

The fully unstructured 2-D mesh used by FUN3D has 3,361 points on the surface and 225 points for the outer farfield of the boundary. The initial off-surface spacing of all meshes is 10^{-6} chord lengths and the extent of the outer domain is 20 chord lengths from the center of the airfoil.

OVERFLOW Code

Another URANS method applied in this study is the OVERFLOW solver [23,24]. A range of turbulence models are available; this work applied both RANS (Menter $k\omega$ -SST) [14] and hybrid RANS/LES (GT-HRLES) [2,5,25] turbulence methodologies. The hybrid RANS/LES method includes a subgrid model based on the solution of the k turbulence equation, and applies the Menter $k\omega$ -SST turbulence model in the computational domain where the flow is not separated. A diagonalized Beam-Warming scalar pentadiagonal scheme with Newton subiterations provides second-order-accurate temporal integration. A fourth-order central difference spatial discretization is combined with a generalized thin-layer Navier-Stokes dissipation scheme to provide algorithm stability. This effort included simulations characterized by fully-turbulent, fixed transition and free transition. Free transition was predicted with the Langtry-Menter (L-M) transition model [26].

Numerical options and grids were based on prior studies using the VR-7, NACA 0012, and SC1095 airfoils and wings [7, 8, 27]. The airfoil configurations modeled the wind tunnel walls via an inviscid boundary condition. The OVERFLOW solver used an overset grid approach with an O-grid (811 × 200 points) for the airfoil, and two Cartesian grids for the wake (204 × 101 points) and tunnel walls (465 × 141 points).

The overset viscous airfoil grids included 35-50 points in the boundary layer with a $y^+ < 1$ at all surface locations. Varying nondimensional time steps per cycle with 10-20 mean transport subiterations and 1-8 additional turbulent transport subiterations have been applied to reduce the residuals and resolve the boundary layer.

VIS07 Code

The VIS07 code is a RANS-Viscous-Inviscid Interaction (VII) approach developed by Le Balleur [28,29]. This RANS-VII is an enhancement of prior VII methods as it can indirectly solve the full RANS equations. It discretizes the RANS (or quasi-RANS) equations using two overlaying adaptive grids and two coupled schemes, where both grids and schemes operate on the same CFD domain. The “Defect Formulation” splitting [28,29] discretizes “Euler” on one grid, and “RANS minus Euler” on the other grid which is self-adaptive in the normal direction to the local viscous layer whether the flow is attached or separated. Both grids have coincident (adaptive) nodes in the streamwise direction along the airfoil wall and wake center-line. Two C-grids grids of 441×100 and 441×61 were used for the inviscid and viscous regions, respectively.

The present version of VIS07 includes new developments not given in Refs. 28 and 29. The Euler field is now projected on the viscous grid at each coupling iteration, discretizing the full “Defect Formulation”. The VII interaction then performs a “field” coupling, not simply a “boundary condition” coupling. The turbulence modeling includes a “ $k - u'v'$ forced” model [29,30] to account for streamline curvature, and a parametric mean velocity profile model [28,29], applied in the direction normal to the “interacted inviscid streamlines.” The self-adaptation of the grids (viscous and inviscid) in the streamwise direction now automatically captures the “physical scales” of the compressions at all phenomena of strong interaction (bubbles, transitions, shocks, turbulent separations, wake rear-stagnations). Transitional bubbles involve an original new model. The self-adaptive grid is used for capturing the laminar separation at the exact streamwise scale. The model defines a maximal laminar path beyond separation, based on the local velocity profile and on the distance from separation, then computes a discontinuous transition within separation (a jump towards a separated turbulent status), and finally computes the end of the bubble compression as turbulent.

XFOIL Code

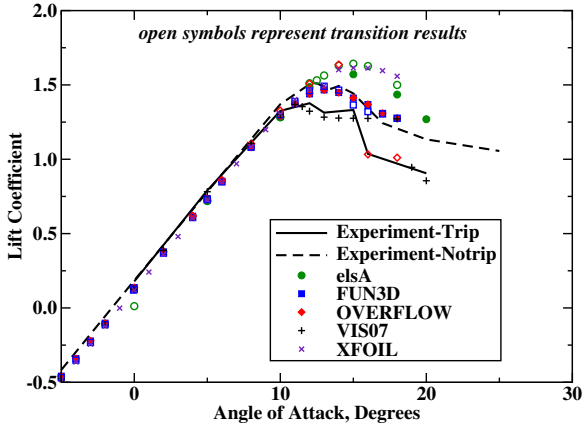
XFOIL [31] is an interactive VII program for the design and analysis of isolated airfoils subjected to steady, subsonic freestream flow. The basic formulation is inviscid and models the flow by utilizing a simple linear-vorticity stream function panel method. Compressibility effects are included by applying the Karman-Tsien compressibility correction which gives good flow predictions up to sonic conditions. The viscous option combines the high-order panel method with a fully-coupled viscous/inviscid interaction method [32]. For the viscous analysis in this study, forced or free transition, transitional separation bubbles, and limited trailing edge separation models were applied.

Grid development for XFOIL reduces to surface panels that

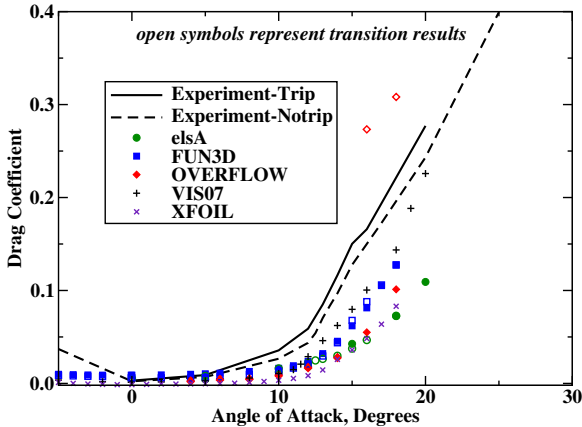
replicate the airfoil shape. Default settings (spacings, numbers of panels, etc.) in XFOIL were utilized for the grids resolved in this analysis.

RESULTS

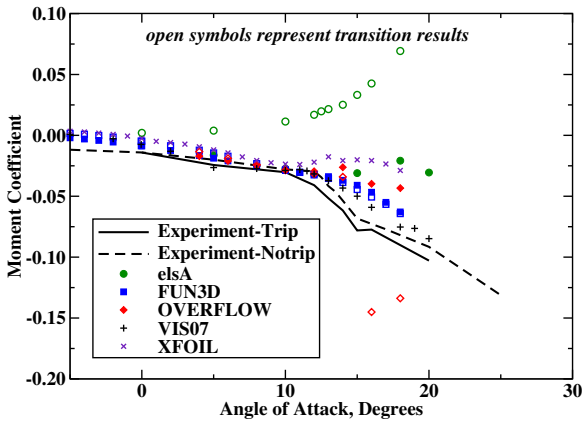
The effects of transition were analyzed for both static and dynamic stall of the VR-7 airfoil. Experimental data from Refs. 9–11 were used for correlation. The VII analyses from VIS07 and XFOIL augmented the static data. It should be noted that only the OVERFLOW calculations modeled wind tunnel walls; however, these effects were negligible.



(a) Lift Coefficient



(b) Drag Coefficient



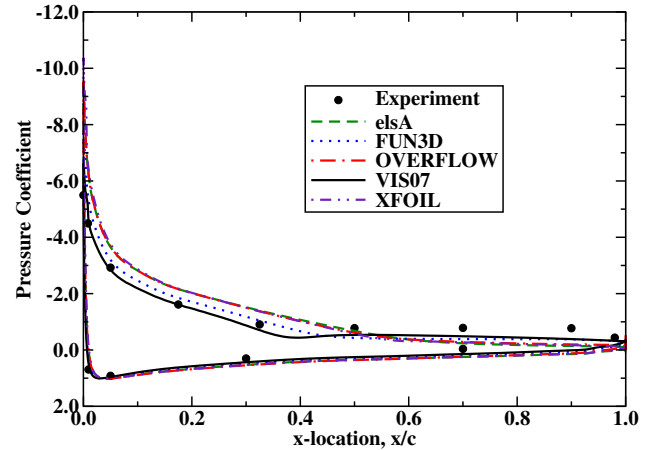
(c) Pitching Moment Coefficient

Figure 1: Static integrated forces and pitching moments for the VR-7 airfoil at $M_\infty=0.185$.

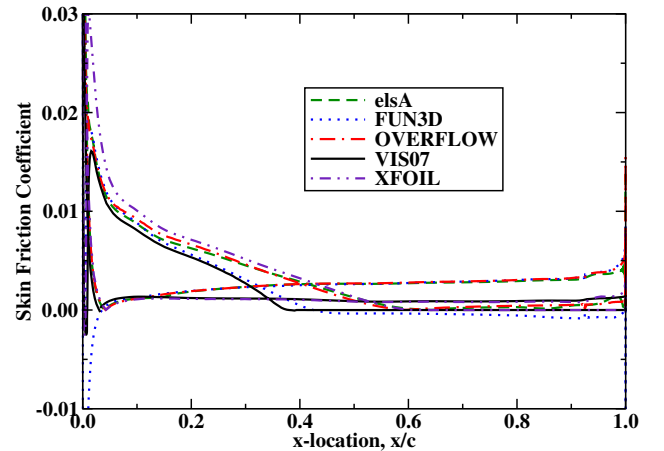
Static Stall

Turbulent flow over the VR-7 airfoil section at increasing angles of attack through static stall at a Mach number of 0.185 and Reynolds number of 2.56 million were computed with the CFD and VII codes. Predicted force and moment coefficients are compared to experimental data in Fig. 1. Experimental data indicate that the influence of transition is to reduce the magnitude of the maximum lift coefficient and the drag rise, with negligible effect on the pitching moment. Fully-turbulent CFD results over-predict the maximum lift coefficient magnitude and location, which also translates into delayed drag rise and pitching moment response at stall.

As expected, for pre-stall cases, the predicted fully-turbulent CFD and VII results correlate well with one another and experimental data, see Fig. 1. However, the predicted post-stall cases exhibit scatter when compared to each other and data. Figure 2 compares the computed pressure and skin friction coefficients using these different methods at the post-stall angle of 15° . The VIS07 and XFOIL simulations included free transition predictions, see Fig. 3 for the predicted transition locations. In spite of the similar transition locations predicted by each of these VII methods, their pressure and skin friction coefficient predictions varied. The cause of the large variation in the post-stall region is not yet known.



(a) Pressure Coefficient



(b) Friction Coefficient

Figure 2: Fully turbulent static pressure and friction coefficients for the VR-7 airfoil at $M_\infty=0.185$ and $\alpha=15^\circ$.

Interestingly, VIS07 and FUN3D agree well with the exper-

imental data on the upper surface, especially prior to 40% chord, in contrast to the other CFD methods and XFOIL. The skin friction plots indicate that the FUN3D and VIS07 methods predict separation at approximately 40% chord, while the remainder of the analyses predict separation near 60% chord. The close correlation of the FUN3D data with VIS07 was not observed at the higher Mach number of 0.30. FUN3D applied the Spalart-Allmaras turbulence model, while the remaining CFD methods applied the Menter $k\omega$ -SST model. The Spalart-Allmaras model is known to be dissipative, and it appears that the good FUN3D correlation for the Mach 0.185 case may be serendipitous due to the combination of the numerics (grid, time step) with the turbulence model. Further analysis is required to confirm this hypothesis.

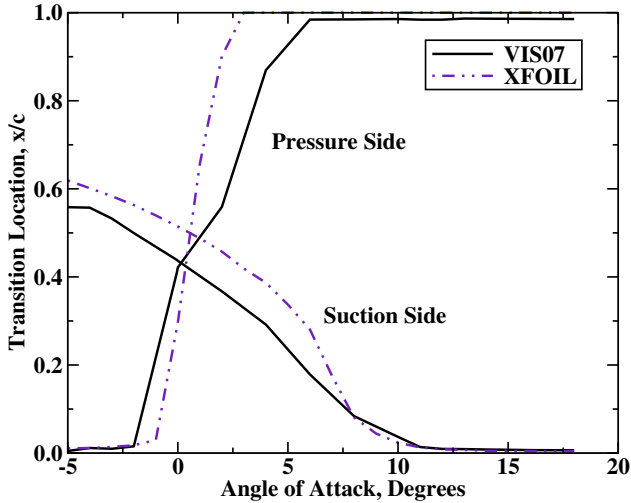
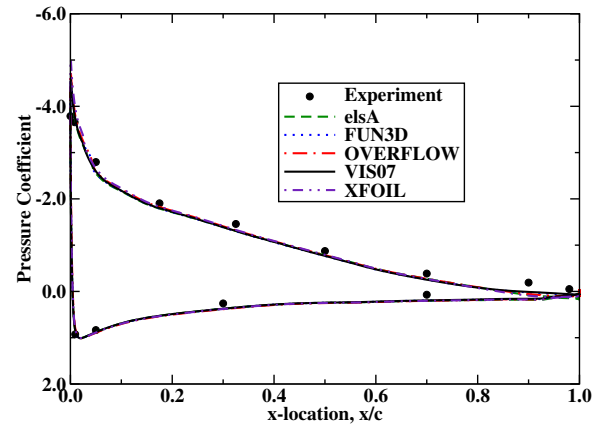


Figure 3: Transition location predictions by XFOIL (dashed lines) and VIS07 (solid lines) for the VR7 airfoil at $M_\infty=0.185$.

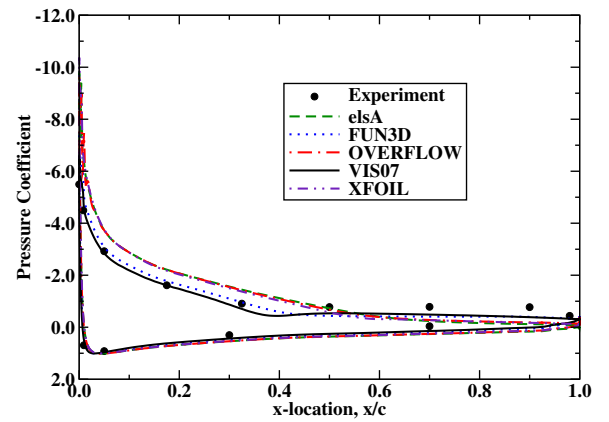
Given these observations, the differences in post stall were attributed to the lack of transitional prediction capability in the CFD methods. In order to address the effect of transition on the airfoil, the transitional locations predicted by the VIS07 method (Fig. 3) were imposed on elsA, OVERFLOW and FUN3D as a fixed, *a priori* defined transition on the suction and pressure sides of the airfoil. As with the fully-turbulent predicted results, shown in Fig. 1, minimal differences in the CFD predictions were observed in the integrated forces and moments when transition was applied. Additional examination using the free transition methods in OVERFLOW and elsA also did not demonstrate changes in the integrated forces and moments. Further examination of the pressure coefficients with fixed transition (FUN3D and OVERFLOW) or free transition (elsA and XFOIL, VIS07) also exhibit minimal changes in both pre- and post-stall angles of attack, see Fig. 4.

These results indicate that it is not only the transition location that matters, but also the manner in which transition is modeled in the RANS CFD methods. For fixed transition, there is typically a binary switch from laminar to turbulent flow. Thus, the influence of the intermittency combined with the statistical modeling of the turbulence appears to be an important key to capturing the physical behavior of the boundary layer when separation is present.

An examination of the velocity profiles at pre- and post-stall conditions in Fig. 5 confirms the behavior noted in the prior discussion. At pre-stall angles of attack, as illustrated by the 10° angle of attack case, only minor differences are noted in the velocity profiles along the upper surface until the trailing edge. At $\alpha = 10^\circ$, the incipient trailing edge separation is not yet evident in the OVERFLOW and XFOIL predictions. For the post-stall conditions, exemplified at $\alpha = 15^\circ$, the velocity profiles are significantly different. At $x/c = 0.3$, VIS07, followed by FUN3D, is clearly closer to separation than the other CFD methods. At $x/c = 0.4$, VIS07 shows separation with some reverse flow, while FUN3D is close to separation. The other methods still exhibit attached profiles. At $x/c = 0.9$, all of the methods indicate that the flow is separated, although the extent of the separated flow above the airfoil varies across the methods.



(a) $\alpha = 10^\circ$



(b) $\alpha = 15^\circ$

Figure 4: Fixed (FUN3D and OVERFLOW) and free transition (elsA, VIS07, XFOIL) pressure coefficients for the VR7 airfoil at $M_\infty=0.185$.

Liggett and Smith [7] have noted the importance of convergence of the boundary layers for time accurate, separated flows. Therefore, both FUN3D and OVERFLOW simulations were repeated with increased turbulent transport subiterations. While some change due to improved convergence was noted in the velocity profiles, there was not a significant change from attached to separated flow. Indeed, the FUN3D predictions shifted closer to the other CFD methods, away from experiment and VIS07 predictions with increased convergence.

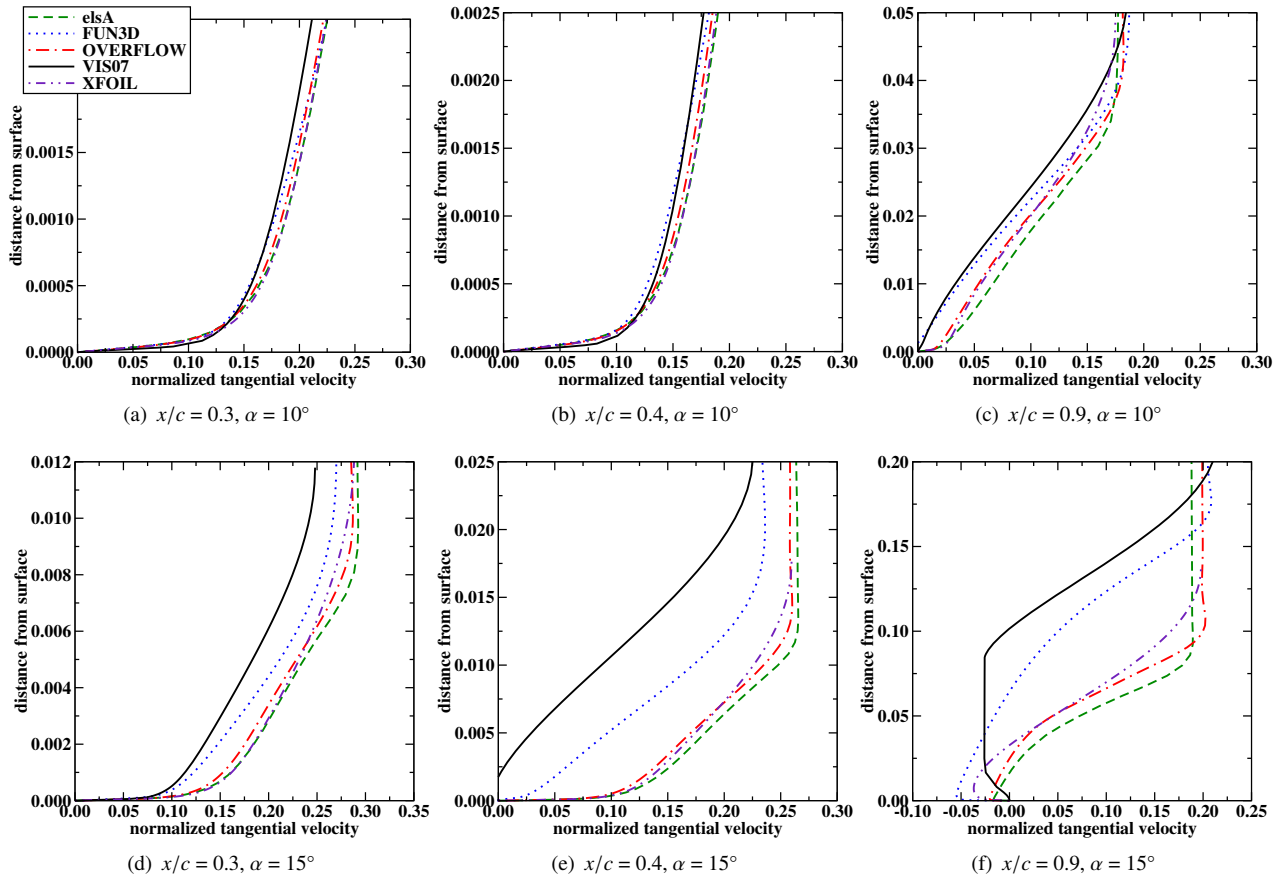


Figure 5: Fixed (FUN3D and OVERFLOW) and free transition (elsA , VIS07, XFOIL) upper surface velocity profiles for the VR7 airfoil at $M_\infty=0.185$.

Dynamic Stall

A number of numerical studies have examined various aspects of grid convergence, turbulence modeling, and temporal integration for application to dynamic stall calculations, as discussed earlier. For this effort, a complex dynamic stall condition that includes a double stall and reattachment with free transition was analyzed. The best practices of these prior studies were utilized here in an attempt to understand the role of transition with respect to the myriad other numerical aspects of the simulation that can influence prediction of dynamic stall.

To examine the current capabilities of CFD and the influence of various numerical options on dynamic stall predictions, consider Fig. 6. Here, a FUN3D two-dimensional simulation with the $k\omega$ -SST turbulence model for 2,000 time steps per cycle with a variable error controller to ensure a residual drop of 4 orders of magnitude in the subiterations of the mean transport equations was applied. OVERFLOW has been run with 6,000 time steps per cycle and 20 mean transport subiterations for a three-dimensional simulation applying a hybrid RANS/LES turbulence method that includes the wind tunnel test section. The elsA simulation applies the $k\omega$ -SST turbulence model for 36,000 time steps per cycle and 10 mean transport subiterations. All are run assuming fully-turbulent conditions.

The behavior of the simulations with regard to several key features of the dynamic stall can be observed. The influence of

the wind tunnel walls (OVERFLOW simulation) can be seen by the shift in the slope of the lift during the initial upstroke. On the downstroke, flow reattachment is not captured for the simulations that apply fewer time steps and subiterations per cycle, indicating that a larger number of the time steps per cycle \times subiterations is needed to *physically* converge the simulation, as discussed by Ref. 7.

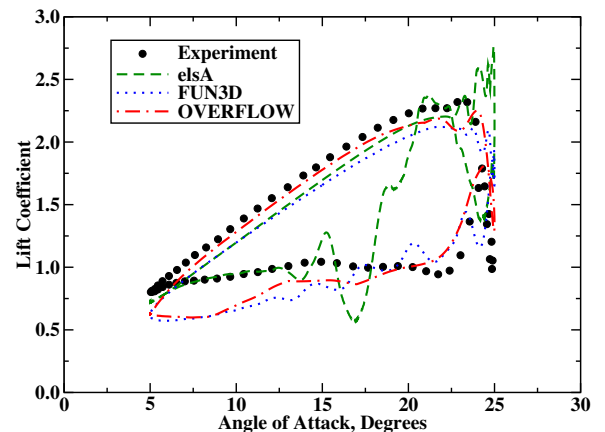


Figure 6: Predicted fully turbulent lift coefficient for the dynamic stall at $M_\infty=0.185$ and $k = 0.1$.

All of the CFD solvers predict stall onset $0.5^\circ - 2^\circ$ higher than the experiment. This is most likely attributed to the question of the tab placement [8]. elsA has a much larger pre-stall lift excursion; this behavior is replicated by OVERFLOW

when it is run with the same temporal integration and turbulence model. The behavior of the double stall appears to be related, at least in part, to the selection of the turbulence method and temporal integration. The hybrid RANS/LES method provides the best prediction of the double dynamic stall, considering both phase and amplitude [8], compared to the RANS model. elsA, with the nominally converged simulation, shows a tendency with the $k\omega$ -SST model to overshoot the double stall, although similar predictions with OVERFLOW show a closer correlation to the hybrid RANS/LES prediction.

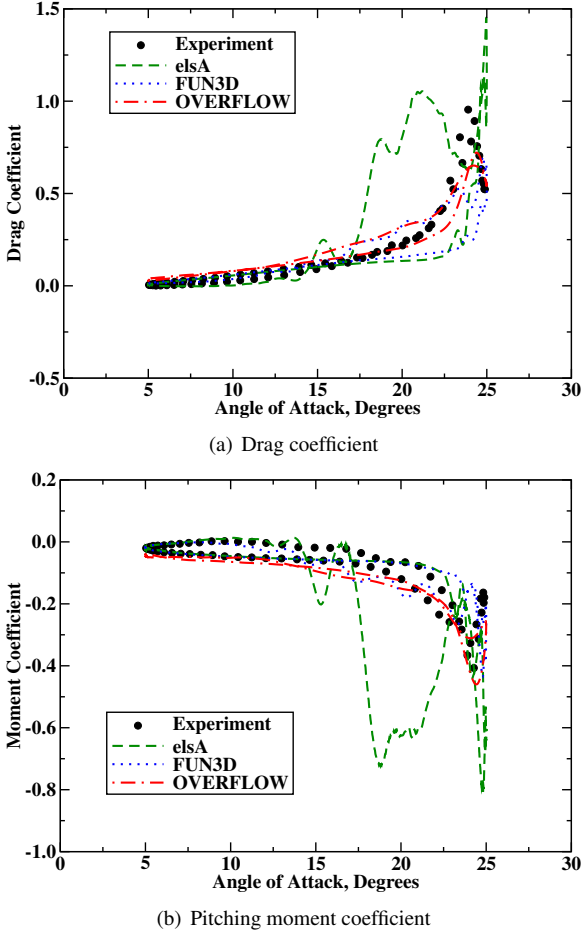


Figure 7: Predicted fully turbulent drag and pitching moment coefficients for the dynamic stall at $M_\infty=0.185$ and $k = 0.1$.

Investigation into the differences between these predictions has focused on temporal integration and the turbulence model. When OVERFLOW is run in two dimensions with the Menter $k\omega$ -SST turbulence model, the overshoot and phase lag observed with the elsA predictions can be partially reproduced. With 9,000 time steps per cycle combined with 20 mean transport subiterations per time step and 4 turbulent transport subiterations per mean subiteration, the behavior of the hysteresis curves predicted by the two solvers are similar. The large overshoot at the stall onset is also observed, particularly for the free transition option in OVERFLOW. When the temporal integration is identical to that of the elsA simulation, as illustrated by the lift coefficient in Fig. 8, the magnification of the second dynamic stall features are mitigated. These temporally refined results approach those that were obtained by the hybrid RANS-LES method observed in Figs. 6 and 7. Simi-

lar improvements in the drag and moment predictions are also observed.

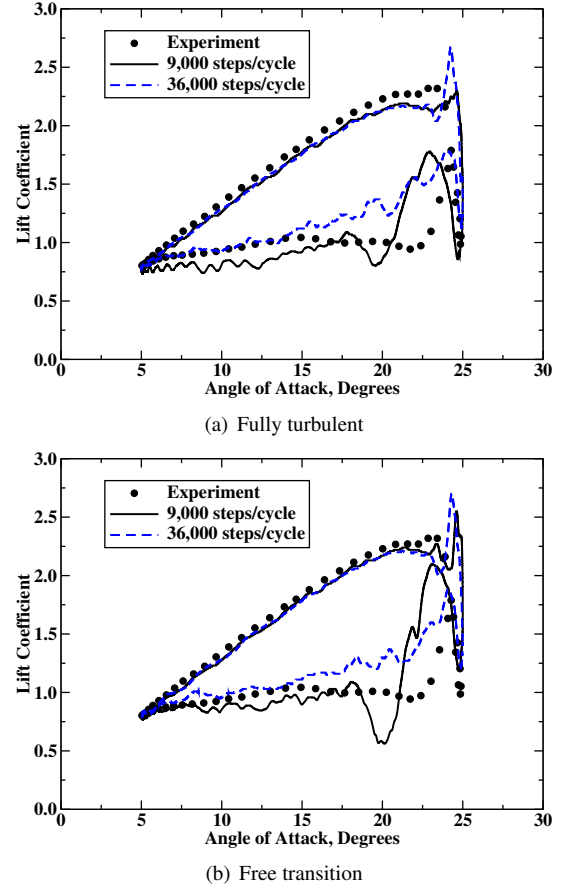
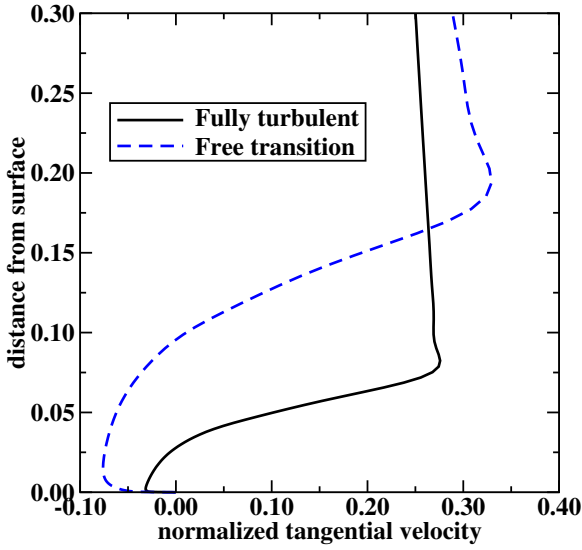


Figure 8: Influence of temporal integration on two-dimensional lift coefficient for the dynamic stall using the OVERFLOW solver and the Menter $k\omega$ -SST turbulence model at $M_\infty=0.185$ and $k = 0.1$.

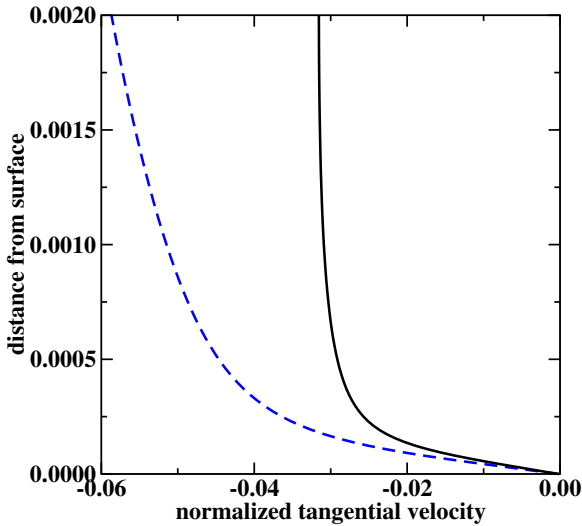
Examination of the velocity profiles adjacent to the airfoil indicates that the boundary layer has not yet converged with the 180,000 timestep \times subiteration combination. This is illustrated by the velocity profiles during the second dynamic stall event in Fig. 9. The magnitude of the reverse flow at the viscous wall and the extent of the separated region is under-predicted when fewer time steps are applied.

The dynamic stall predictions were then evaluated using two different transition models: the Langtry-Menter model in OVERFLOW and the AHD-lsb model in elsA. Both the OVERFLOW and elsA simulations included 36,000 time steps with 10 mean and turbulent transport subiterations per time step for a total of 360,000 time step \times subiterations per cycle. The predicted transition locations on the upper surface for these models are shown in Fig. 10. The location of transition for both methods remains relatively constant within 5% of the leading edge through the initial upstroke and downstroke of the dynamic stall cycle. As the airfoil passes through the mean angle of attack on the downstroke, the transition location moves aft to approximately 30% of the chord for the AHD-lsb model and 40% of the chord for the Langtry-Menter model, see Fig. 10. The extent of the transition location during the downstroke appears to have a secondary influence on the recovery; the primary behavior is still governed by the behavior of the turbu-

lence model. This may be a function of the strong stall in this evaluation case. Richter et al. [6] found that for the OA209 airfoil, the influence of transition depended on the conditions of the dynamic stall, including Mach number and amplitude of oscillation.



(a) Full boundary layer



(b) Surface

Figure 9: Influence of temporal integration on free transition two-dimensional boundary layer at $\alpha=23.66^\circ$ down for the dynamic stall using the OVERFLOW solver and the Menter $k\omega$ -SST turbulence model at $M_\infty=0.185$ and $k = 0.1$.

Examining the integrated forces (Figs. 11 and 12) and pitching moment (Fig. 12) with and without transition, it is clear that the influence of transition in two-dimensional dynamic stall using the $k\omega$ -SST turbulence model is minimal for the OVERFLOW simulation. For the elsA simulation, it influences primarily the location of the stall onset, as well as the phase and recovery of the secondary stall. elsA predicts an abrupt stall with fully turbulent flow, but the stall becomes less abrupt, and more comparable to the behavior of the experimental stall onset when transition is applied. The change in the character of the stall onset is not observed in the OVERFLOW results. The elsA simulations was also able to capture the cross-over behavior observed in experiments during the

first dynamic stall event, albeit $3/4^\circ$ earlier than experiment.

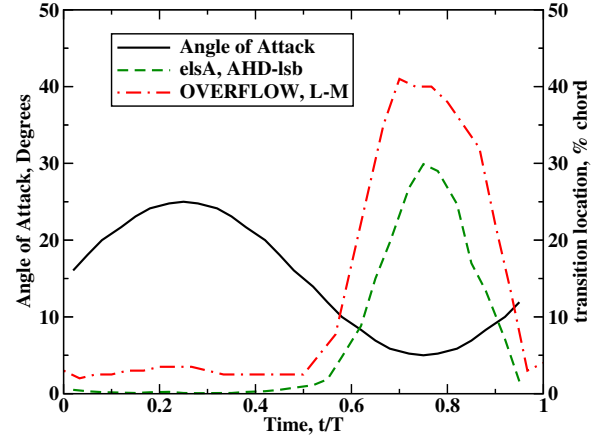
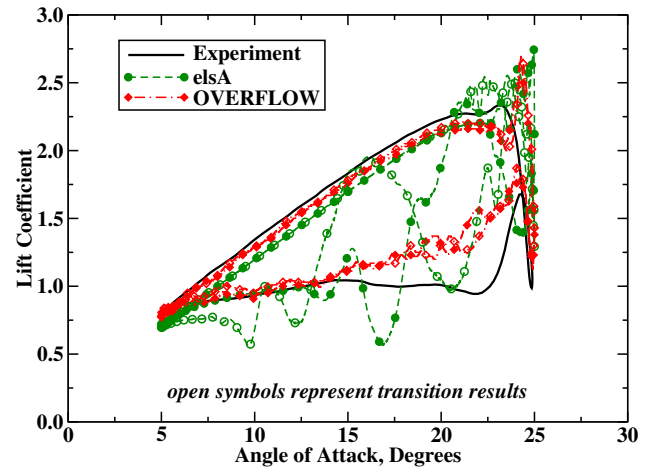
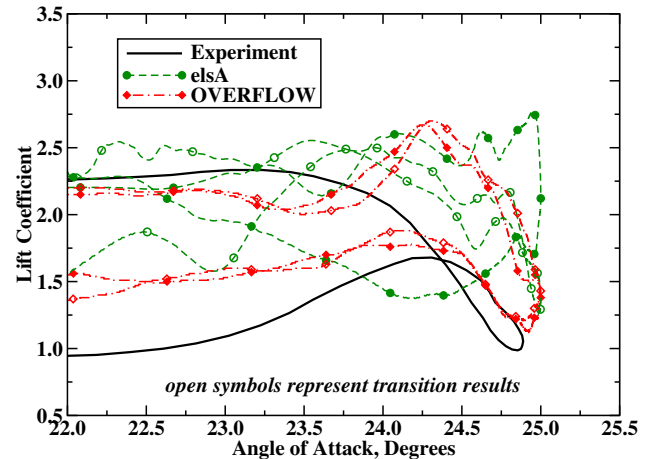


Figure 10: Predicted transition location along the upper surface of the dynamic stall airfoil.

When OVERFLOW was run at the lower number of time steps \times subiterations per cycle (Fig. 8), it was observed that the phase of the secondary stall was shifted closer toward experiment by approximately 1° , but still includes a 1-1.5 $^\circ$ lag. The overshoot of the secondary stall magnitude and its recovery is not influenced by transition, nor is the location of stall onset.

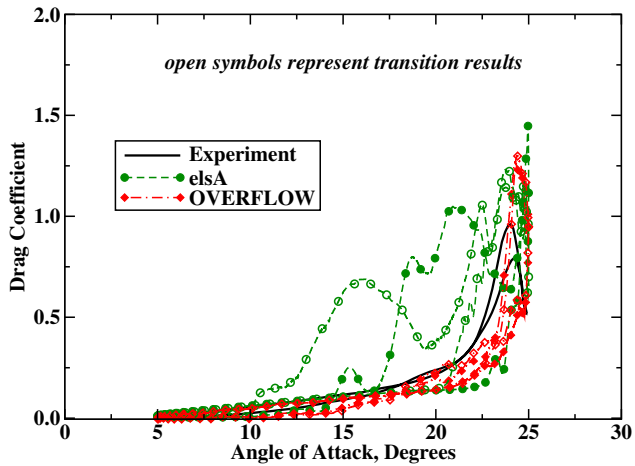


(a) Lift coefficient

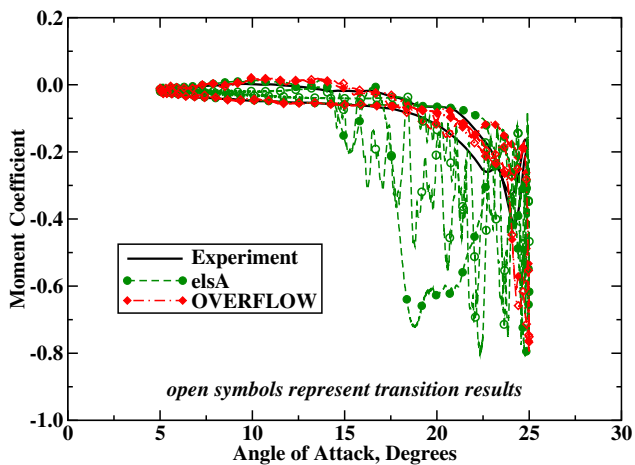


(b) Expanded Lift coefficient

Figure 11: Fully turbulent and free transition lift coefficient for dynamic stall at $M_\infty=0.185$ and $k = 0.1$.



(a) Drag coefficient



(b) Pitching moment coefficient

Figure 12: Fully turbulent and free transition performance for dynamic stall at $M_\infty=0.185$ and $k = 0.1$.

The differences in the predicted dynamic stall physics with and without transition can be observed by comparing the velocity profiles during dynamic stall (Figs. 13 and 14). At stall onset (Fig. 13a), transition predicts a stronger reverse flow on the forward portion of the airfoil upper surface, while the opposite is true near the trailing edge. The extent of the separated flow normal to the surface is larger when transition is present.

At the maximum angle of attack, which is the location where lift once again increases, transition plays a larger role (Fig. 13b). Here the degree of separation or reverse flow is mitigated with transition at the extrema of the airfoil chord. The vortex at the trailing edge has been shed, as indicated by the tangential velocity profile above the airfoil. The vortex in the fully turbulent simulation has not yet been fully shed from the airfoil, producing the local reverse flow at the $x/c=0.9$ location.

During the second stall event, the velocity profiles in Fig. 14 indicates that transition primarily influences the extent of the velocity deficit above the airfoil, with smaller impact at the surface. The mean velocity is recovered at almost twice the normal distance from the forward airfoil surface when transition is present. Near the trailing edge at $x/c=0.9$, transition

results in an attached rather than separated boundary layer as stall is approached ($\alpha=24.5^\circ$ down) or, conversely, a stronger region of reversed flow during the angle of attack reduction post stall.

CONCLUSIONS

This paper has explored the use and efficacy of prescribed transition models in the prediction of static and dynamic stall on the VR-7 airfoil. Experimental data provided of correlation of integrated loads, and viscous-inviscid interaction solvers were used to aid in the characterization of the boundary layer in attached and separated flows for static conditions. Spatial and temporal studies previously carried out by the authors and others are leveraged to examine the causal influences of the numerical and physical artifacts of the simulations. From these static and dynamic analyses of the VR-7 airfoil, the following observations for transition in CFD solvers can be reached:

1. Free and fixed (defined *a priori* to static simulations) transition, provide excellent correlation with experiment when the flow is attached.
2. Fixed and free (AHD-lsb and Langtry-Menter models) transition in static stall conditions where separated flow is present do not provide the expected influence in pressure coefficient aft of the transition location observed in experimental results and some viscous-inviscid solvers. The influence of the turbulence modeling downstream of the transition location needs to be further studied, in particular when the transition from laminar to turbulent flow is modeled as a step function.
3. Free transition predictions using the Langtry-Menter and AHD-lsb methods, indicated minor success in improving the prediction of the double dynamic stall. This improvement was most apparent when the simulation was not fully converged temporally.
4. The primary influence in the prediction of the dynamic stall is the temporal convergence of the boundary layers, which is prescribed by the turbulence methodology applied in the simulations.

Further analysis is warranted to include transition with the hybrid RANS/LES turbulence method, and to extend this analysis to other airfoils and dynamic stall conditions. The examination of other transition methods may also provide further insights in the physics of flow separation.

ACKNOWLEDGMENTS

The views and conclusions contained in this document are those of the authors and should not be interpreted as representing the official policies, either expressed or implied, of the AMRDEC (Aviation and Missile Research, Development and Engineering Center) or the U.S. Government. The U.S. Government is authorized to reproduce and distribute reprints for Government purposes notwithstanding any copyright notation thereon.

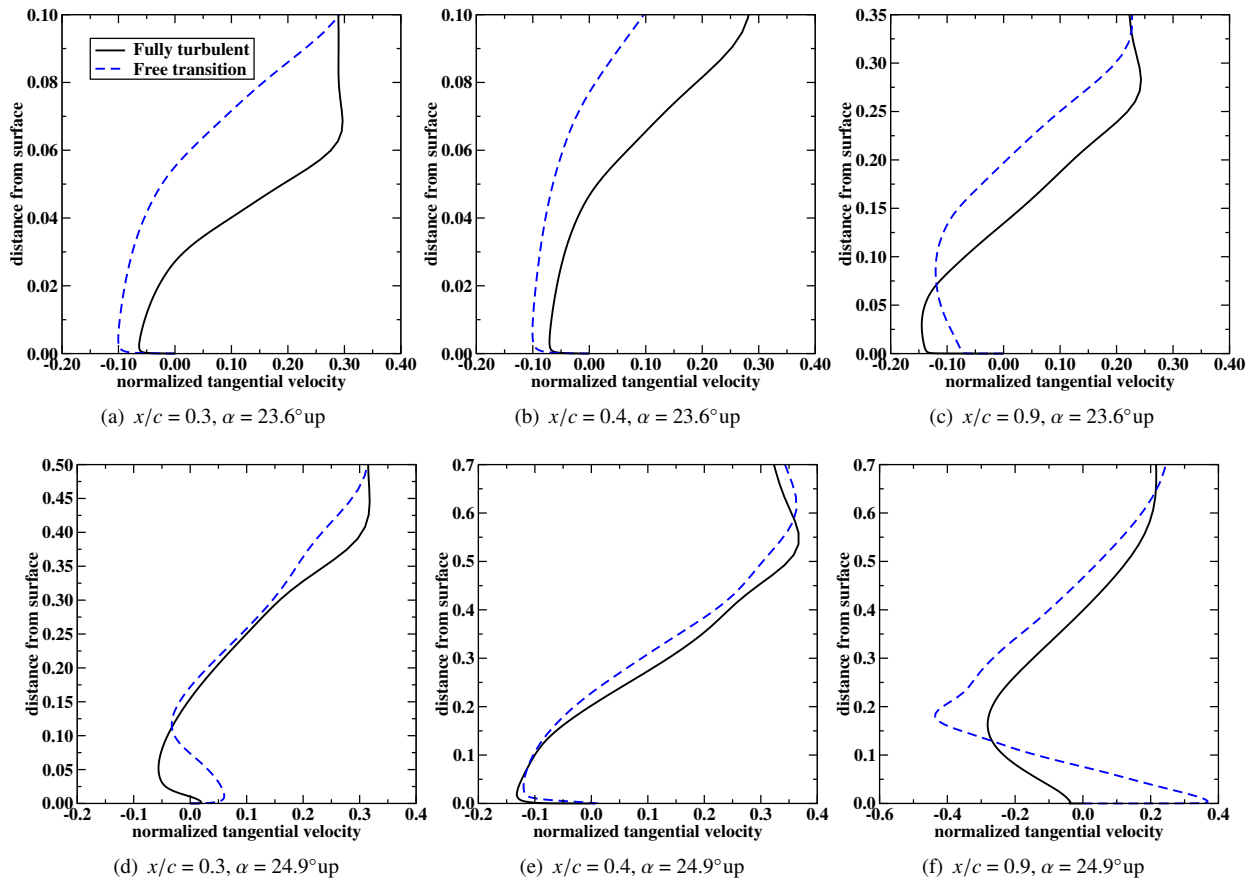


Figure 13: Fully turbulent and free transition (Langtry-Menter model) upper surface velocity profiles for the VR7 airfoil for the first dynamic stall event at $k=0.1$ and $M_\infty=0.185$.

Computational support was provided through the DoD High Performance Computing Centers at ERDC through an HPC grant from the US Army. Any opinions, findings, and conclusions or recommendations expressed in this material are those of the author(s) and do not necessarily reflect the views of the Department of the Army.

The authors would like to especially acknowledge and thank Christopher Sandwich, Nicholas Liggett, and Jean de Montaudouin for help in submitting runs and post-processing data for some of the computations.

References

- [1] Smith, M., Wong, T., Potsdam, M., Baeder, J., and Phanse, S., "Evaluation of CFD to Determine Two-Dimensional Airfoil Characteristics for Rotorcraft Applications," *Journal of the American Helicopter Society*, Vol. 50, (1), 2006, pp. 70–79.
- [2] Sanchez-Rocha, M., Kirtas, M., and Menon, S., "Zonal Hybrid RANS-LES Method for Static and Oscillating Airfoils and Wings," AIAA 2006-1256, 44th AIAA Aerospace Sciences Meeting, Reno, NV, January 2006.
- [3] Gleize, V. and Szydowski, J. and Costes, M., "Numerical and Physical Analysis of the Turbulent Viscous Flow Around a NACA0015 Profile at Stall," European Congress on Computational Methods in Applied Sciences and Engineering, Jyväskylä, Finland, 2004.
- [4] Szydowski, J. and Costes, M., "Simulation of flow around NACA 0015 airfoil for static and dynamic stall configurations using RANS and DES," *Tiré à part- Office national d'études et de recherches aérospatiales*.
- [5] Shelton, A. B., Braman, K., Smith, M. J., and Menon, S., "Improved Hybrid RANS-LES Turbulence Modeling for Rotorcraft," American Helicopter Society 62nd Annual Forum Proceedings, Phoenix, AZ, May 9-11, 2006.
- [6] Richter, K., Le Pape, A., Knopp, T., Costes, M., Gleize, V., and Gardner, A., "Improved Two-Dimensional Dynamic Stall Prediction with Structured and Hybrid Numerical Methods," *Journal of the American Helicopter Society*, to appear, 2011.
- [7] Liggett, N. and Smith, M., "Temporal Convergence Criteria for Time-Accurate Viscous Simulations of Separated Flows," *Computers & Fluids*, submitted July, 2011.
- [8] Moulton, M. A. and Smith, M. J., "The Prediction and Validation of Static and Dynamic Stall," Heli Japan 2010, Saitama, Japan, November 2010.
- [9] McCroskey, W. J., McAlister, K. W., Carr, L. W., and Pucci, S. L., "An Experimental Study of Dynamic Stall on Advanced Airfoil Sections Volume 1. Summary of the

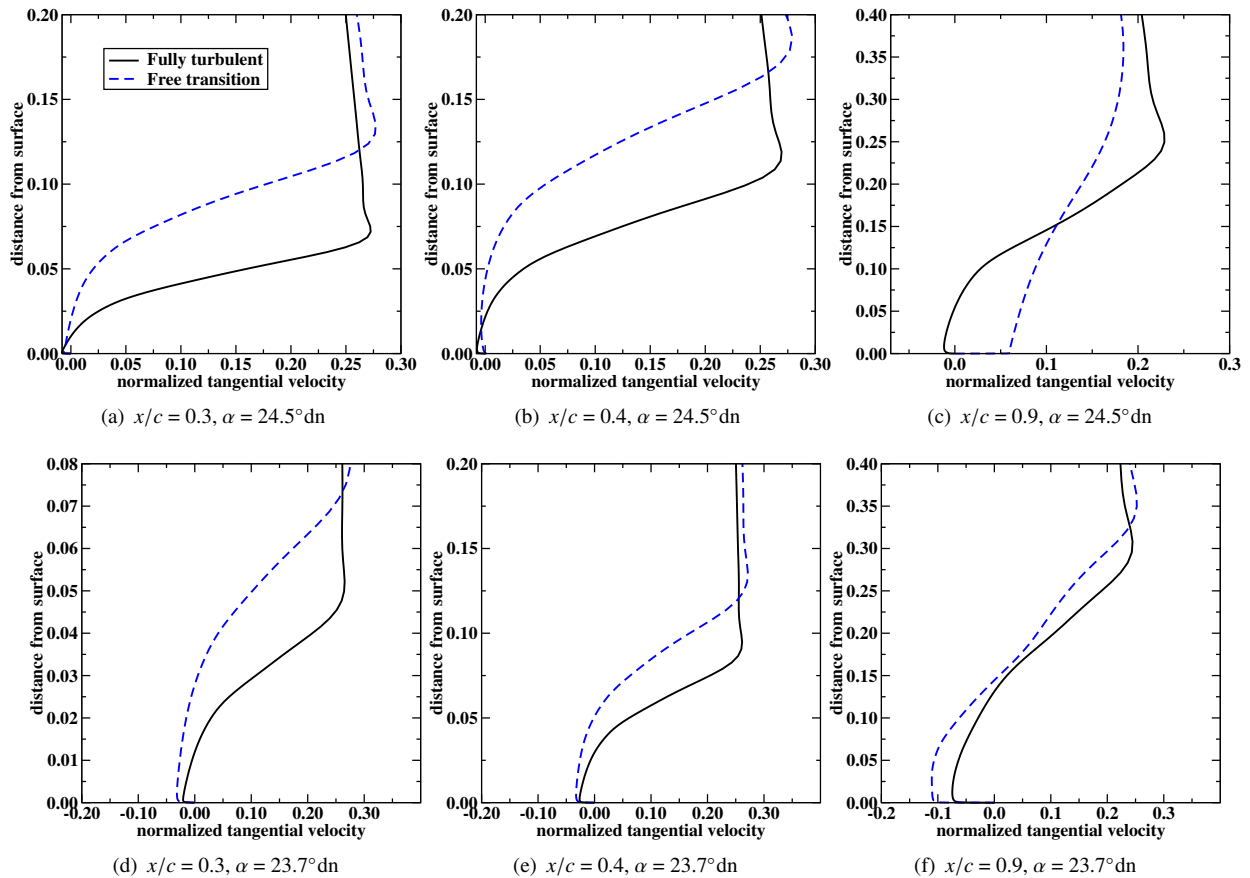


Figure 14: Fully turbulent and free transition (Langtry-Menter model) upper surface velocity profiles for the VR7 airfoil for the second dynamic stall event at $k=0.1$ and $M_\infty=0.185$.

- Experiment,” Technical Report NASA TM 84245 (US-AAVRADCOM TR-82-A-8), US Army AVRADCOM, July 1982.
- [10] McAlister, K. W., Pucci, S. L., McCroskey, W. J., and Carr, L. W., “An Experimental Study of Dynamic Stall on Advanced Airfoil Sections Volume 2. Pressure and Force Data,” Technical Report NASA TM 84245 (US-AAVRADCOM TR-82-A-8), US Army AVRADCOM, September 1982.
- [11] Carr, L. W., McCroskey, W. J., McAlister, K. W., Pucci, S. L., and Lambert, O., “An Experimental Study of Dynamic Stall on Advanced Airfoil Sections Volume 3. Hot-Wire and Hot-Film Measurements,” Technical Report NASA TM 84245 (USAAVRADCOM TR-82-A-8), US Army AVRADCOM, December 1982.
- [12] Cambier, L., Gazaix, M., Heib, S., Plot, S., Poinot, M., Vuillot, J.-P., Bousuge, J.-F., and Montagnac, M., “An Overview of the Multi-Purpose elsA Flow Solver,” *Aerospace Lab*, Issue 2, 2011.
- [13] Edwards, J. and Liou, M., “Low-diffusion flux-splitting methods for flows at all speeds,” *AIAA Journal*, Vol. 36, 1998, pp. 1610–1617.
- [14] Menter, F., “Two-Equation Eddy-Viscosity Turbulence Models for Engineering Applications,” *AIAA Journal*, Vol. 32, (8), August 1994, pp. 1598–1605.
- [15] Arnal, D., Habiballah, M., and Coustols, E., “Laminar instability theory and transition criteria in two- and three-dimensional flows,” *La Recherche Aérospatiale N°*, 1984-2, 1984.
- [16] Roberts, K., “The effect of Reynolds number and laminar separation on axial cascade performance,” *ASME Journal of Engineering for Gas Turbines and Power*, Vol. 97, 1975, pp. 261–274.
- [17] Gleyzes, C., Cousteix, J., and Bonnet, J., “A calculation method of leading edge separation bubbles,” *Numerical and Physical Aspects of Aerodynamic Flows*, Vol. II, Springer Verlag, 1984.
- [18] Richez, F., Gleize, V., Mary, I., and Basdevant, C., “Zonal RANS/LES coupling simulation of a transitional and separated flow around an airfoil at high angle of attack,” *EUROMECH Colloquium 469*, Dresden, Germany, October 2005.
- [19] Gleize, V., Le Pape, A., Costes, M., and Richez, F., “Numerical simulation of a pitching airfoil under dynamic stall conditions including laminar/turbulent transition,” *AIAA paper 2008-0391*, 46th Aerospace Sciences Meeting and Exhibit, Reno, NV, January 7-10, 2008.
- [20] Biedron, R. T., Vatsa, V. N., and Atkins, H. L., “Simulation of Unsteady Flows Using an Unstructured Navier-Stokes Solver on Moving and Stationary Grids,” *AIAA Paper 2005-5093*, June 2005.

- [21] Spalart, P. and Allmaras, S., "A one-equation turbulence model for aerodynamic flows," AIAA, Aerospace Sciences Meeting and Exhibit, 30 th, Reno, NV, 1992, p. 1992.
- [22] Vatsa, V. N. and Carpenter, M. H., "Higher Order Temporal Schemes with Error Controllers for Unsteady Navier-Stokes Equations," AIAA Paper 2005-5245, 2005.
- [23] Buning, P., Chiu, I., Obayashi, S., and Steger, J., "Numerical Simulation of the Integrated Space Shuttle Vehicle in Ascent," AIAA 88-4359, AIAA Atmospheric Flight Mechanics Meeting, Minneapolis, MN, August 1988.
- [24] Meakin, R., "Moving Body Overset Grid Methods for Complete Aircraft Tiltrotor Simulations," 11th AIAA Computational Fluid Dynamics Conference, AIAA-1993-3350, Orlando, FL, July 6-9, 1993.
- [25] Liggett, N. and Smith, M., "Cavity Flow Assessment Using Advanced Turbulence Modeling," AIAA 2010-1200, 48th AIAA Aerospace Sciences Meeting Including the New Horizons Forum and Aerospace Exposition, Orlando, FL, January 2010.
- [26] Langtry, R. B. and Menter, F. R., "Correlation-Based Transition Modeling for Unstructured Parallelized Computational Fluid Dynamics Codes," *AIAA Journal*, Vol. 47, (12), 2009, pp. 2894–2906.
- [27] Smith, M. and Liggett, N. and Koukol, B., "The Aerodynamics of Airfoils at High and Reverse Angles of Attack," *Journal of Aircraft*, to appear, 2011.
- [28] Le Balleur, J.-C., "Viscous-inviscid calculation of high-lift separated compressible flows over airfoils and wings," Proceedings AGARD CP 515, 1993, paper 26, Banff, Canada (see also ONERA TP 1992-184).
- [29] Le Balleur, J.-C., "New possibilities of viscous-inviscid numerical techniques for solving viscous flow equations with massive separation," 4th symposium numerical/physical aspects of aerodynamic flows, Springer Verlag 1990, p.71-96, ed. T. Cebeci (see also ONERA TP 1989-24).
- [30] Le Balleur, J.-C., "Numerical viscous-inviscid interaction in steady and unsteady flows," 2nd symposium numerical/physical aspects of aerodynamic flows, Chap. 13, p. 259-284, ed. T. Cebeci, Springer Verlag 1984 (see also ONERA TP 1983-8).
- [31] Drela, M., "XFOIL : An Analysis and Design System for Low Reynolds Number Airfoils," Conference on Low Reynolds Number Airfoil Aerodynamics, University of Notre Dame, June 1989.
- [32] Drela, M. and Giles, M. B., "Viscous-Inviscid Analysis of Transonic and Low Reynolds Number Airfoils," *AIAA Journal*, Vol. 25, (10), October 1987, pp. 1347–1355.